Modulation of dependencies by brain states in a laminar cortical circuit

Anirban Das[2,3,4,#], Alec G. Sheffield[1,#], Anirvan S. Nandy[1,3,†] and Monika P. Jadi[1,2,3,†,*]

[1]Interdepartmental Neuroscience Program, Yale University, New Haven, CT 06511

[2]Department of Psychiatry, Yale University, New Haven, CT 06511

[3]Department of Neuroscience, Yale University, New Haven, CT 06511

[4]Design and Patterning AI Group, Intel Corp., Hillsboro, Oregon 97124

[#]equal contribution

[†]senior author

[*]corresponding author (monika.jadi@yale.edu)

ABSTRACT

Adaptive information processing, comprised of local computations and their efficient routing, is crucial for flexible brain function. Spatial attention is a quintessential example of this adaptive process. It is critical for recognizing and interacting with behaviorally relevant objects in a cluttered environment[1]. Object recognition is mediated by ensembles of computational units distributed across the ventral visual hierarchy. How the deployment of spatial attention aids these hierarchical computations is unclear. Based on pairwise correlation analysis, two key mechanisms have been proposed: First is an improvement in the efficacy of unique information directed from one encoding stage to another, suggested by evidence along the visual hierarchy[2-6]. Based on the theoretical results that even weak correlated variability can substantially limit the encoding capacity of a neuronal pool[7], a second proposal is an improvement in the sensory information capacity of an encoding stage through a reduction in shared fluctuations[8,9]. However, pairwise analyses capture both unique and shared components of fluctuations, and therefore cannot disambiguate the proposed mechanisms. To test these proposals, it is crucial to estimate the

attentional modulation of unique information flow across and shared information within the stages of the visual hierarchy. We investigated this in the multi-stage laminar network of visual area V4, an area strongly modulated by attention[10-12]. Using network-based statistical modeling, we estimated the strength of inter-layer information flow by measuring statistical dependencies that reflect how the cortical layers *uniquely* drive each other's neural activity. We quantified their modulation across attention conditions (attend-in vs. attend-away) in a change detection task and found that deployment of attention indeed strengthened unique dependencies between the input and superficial layers. Using the partial information decomposition framework[13,14], we estimated modulation of shared dependencies and found that they are reduced within laminar populations, specifically the putative excitatory subpopulations. Surprisingly, we found a strengthening of unique dependencies within the laminar populations, a finding not previously predicted. Crucially, these modulation patterns were also observed across behavioral outcomes (hit vs. miss) that are thought to be mediated by endogenous state fluctuations[15-17]. By "decomposing" the modulation of dependency components and in combination with prior theoretical work[7], our results suggest the following computational model of optimal sensory states that are attained by either task demands or endogenous fluctuations in brain state: enhanced information flow *between* and improved information capacity *within* encoding stages.

42 **MAIN TEXT**

43 Visual cortex has a laminar organization and both sensory computations and information flow
44 patterns are layer specific, forming the building blocks of the ventral visual hierarchy[18-22]. We
45 hypothesized that the deployment of spatial attention strengthens unique inter-layer information
46 transfer between and weakens shared information within the input and superficial layers, both of
47 which are crucial nodes of information flow along the ventral visual hierarchy. To test this, our
48 primary goal was to quantify unique statistical spiking dependencies between the populations of
49 each layer, which requires characterizing the joint spiking activity of the laminar ensemble.
50 Cortical ensembles are highly interconnected, and this can be a source of both shared and unique
51 dependencies between any pair of ensemble members (Fig 1a, S1a-b). Pairwise measures (such
52 as correlations) reflect both unique and shared sources of dependences (Fig 1b,c), whereas
53 network-based methods primarily extract non-shared sources of dependencies (Fig 1d). Using
54 the Partial Information Decomposition framework[13,14], we proceeded to use a combination of
55 network-based probabilistic graphical models (PGM)[23] and pairwise regression models to analyze
56 the neurophysiological data and "decompose" the modulation of these dependencies by spatial
57 attention (Fig 1e, see SI Methods). Fitting our data with Dynamic Bayesian Networks (DBN)[24-29],
58 a class of PGMs, allowed unbiased discovery of multi-timescale directed and cyclical
59 dependencies that are Granger causal[30], without making assumptions about their specific nature
60 (linear/nonlinear), direction, or latency (Fig 2a, Fig S2). Directed dependencies are expected to
61 reflect the unique information flow in our data. We estimated the probability of discovered
62 dependencies (referred henceforth as weights of a graph edge) and used it as a measure of their
63 strength[31] (Fig 2a,b). We used a time-shuffled estimate of the edge weights to determine the
64 statistical significance of the discovered dependencies (Fig 2a). We refer to this approach as
65 multi-timescale weighted Dynamic Bayesian Networks (MTwDBN). When tested on a ground truth

66 synthetic network with recurrent connections, MTwDBN approach robustly recovered the
67 dependency structure (Fig 2c-e), and performed significantly better than existing methods,
68 especially when the populations were sparsely sampled (Fig 2f), as is the case in neural
69 recordings[32-34]. Since the dependencies are discovered without assumption of independence
70 between predictors, edge weights in MTwDBN can be interpreted as an accurate depiction of the
71 structure *and* strength of unique dependencies in a highly interconnected network (Fig 2g).
72
73 We applied the MTwDBN analysis to laminar recordings in visual area V4 (an area strongly
74 modulated by attention[8,11,35-37]) of non-human primates performing an attention demanding
75 orientation change detection task (Fig 3a,b; see Methods and Fig S3). We first analyzed the
76 ensemble of layer-wise populations (Fig 3c) and quantified the net attentional modulation of
77 dependencies across different timescales (Fig 3d). At longer timescales (> 60 ms lag)[33], while
78 attention weakened pairwise dependencies, in agreement with previous findings[38,39], we found a
79 strengthening of unique dependencies. This allowed us to infer (Fig 1e) that it is the shared
80 component of dependencies that is weakened by attention (Fig 3d), thereby providing direct
81 evidence for a previously hypothesized mechanism of perceptual improvement by attention[38,39].
82 Directed dependencies between layers, specifically those between the input and superficial
83 layers, an important link in feedforward processing, were strengthened by attention (Fig 3e). On
84 the other hand, shared dependencies within the input and superficial layers were weakened by
85 attention (Fig 3f). Surprisingly, unique dependencies within the layers were strengthened by
86 attention at most timescales (Fig 3g). Taken together, these results provide the first direct
87 evidence that attention improves unique dependencies both within and across stages of the
88 ventral visual hierarchy, while weakening shared dependencies within these stages (Fig 3h).
89

Neuronal cell-classes in the cortex contribute differentially to information processing[35,36,40]. To test if the above model holds when we allow discovery of cell-class specific dependencies, we next analyzed an ensemble of broad- and narrow-spiking layer-wise populations (Fig 3i) and quantified the net attentional modulation of dependencies across different timescales (Fig 3j). The pattern of net modulation of unique and shared dependencies in this ensemble largely mirrored that discovered in the layer-wise aggregated ensemble, specifically at the longer timescales. Same was the case for modulation of unique dependencies between layers and shared dependencies within layers (consistent across both animals) (Fig 3k,l). Theoretical predictions[7], including our hypotheses, regarding effects of shared fluctuations on information representation apply primarily to excitatory neurons. When we quantified the attention modulation of shared dependencies within layers in a cell-class specific manner, we found that the broad-spiking population (putative excitatory neurons) showed a robust weakening of shared dependencies within layers (consistent across animals) (Fig 3l). On the other hand, the narrow-spiking population (putative inhibitory neurons) showed a distinct pattern, one that was dominated by strengthening of shared dependencies within layers. Consistent with the findings in the aggregated ensemble, unique dependencies within the layers were strengthened by attention at most timescales (Fig 3m). Taken together, these results provide the first direct evidence that attention specifically weakens shared dependencies in the projection populations within encoding stages, in addition to robustly improving unique dependencies both within and across stages of the ventral visual hierarchy (Fig 3n).

To test if the pattern of inter- and intra-layer dependency modulation that we observed is a signature of brain states that are optimal for perceptual behavior, we analyzed the laminar ensemble activity for a subset of trials within the attend-in condition in which the animal was equally likely to correctly detect (Hit) or fail to detect (Miss) the orientation change (Fig 4a,b). Controlling for task and stimulus conditions, these behavioral fluctuations are thought to arise

from endogenous fluctuations such as attentive sampling and arousal changes[15-17,41,42]. The pattern of net modulation of unique and shared dependencies across behavioral outcome (Fig 4c) largely mirrored that discovered across attentive states (Fig 3d) at the longer timescales. Same was the case for modulation of unique dependencies between layers and dependencies within layers (Fig 4d), suggesting that the pattern of enhanced inter-layer unique dependencies and weakened intra-layer shared dependencies is a hallmark of brain states that are optimal for perceptual performance (Fig 4e). Combined with prior theoretical work[7], our results suggest a model of enhanced inter-layer communication and improved intra-layer information capacity during optimal states that are either imposed by task demands or are attained via endogenous fluctuations in brain state.

Our approach demonstrates that the information flow structure in a neural ensemble is robustly described by Dynamic Bayesian Network modeling that is adapted to include multiple lags spanning timescales of interest. This unbiased approach allows us to dive deeper into the causal functional interactions (beyond correlations) in a multivariate system with unknown nonlinear dependencies. Further, the results demonstrate that weighing dependencies using confidence measures provides a more accurate information flow structure that can be utilized to investigate how this structure is modulated by changes in brain and behavioral states. Finally, a novel combination of this approach with pairwise models allows decomposition of changes in unique and shared components of dependencies. Since directed unique dependencies suggest causality and shared ones suggest common inputs, this allows us to gain insights into underlying mechanisms. In contrast, prior correlational studies have quantified net dependency modulation, and thus the underlying mechanisms remained hypothetical [2,9,38].

While approaches such as GLM have been very useful in providing improved phenomenological models of individual neural responses to sensory stimulation in early sensory circuits[43], they are not suitable for dependency structure learning in a highly recurrent cortical ensemble. Their inherent assumption of the independence of predictor variables can discover spurious dependencies due to shared inputs, and result in a dense and likely inaccurate structure. Since structure learning in DBNs involves determining conditional independence by solving an optimization problem that penalizes density, our approach is ideal for generating a sparse and hence interpretable unique dependency structure in multivariate data.

This class of DBN models does not identify functional consequences of dependencies between populations, such as enhancement or suppression of target activity. Future work in this direction will further enhance the functional interpretability of discovered dependencies. Nonetheless, these models are effective in elucidating structure and modulation of information flow in a multivariate system such as the laminar cortical network.

In general, discovery of dependency structure using our approach is sensitive to the inclusion of relevant neural variables. It is indeed possible that a gross classification of subpopulations as broad and narrow in our study fuses distinct but relevant neural variables. On the other hand, our three and six population laminar DBNs yield consistent patterns regarding modulation of dependencies, suggesting an inclusion of relevant variables for the purposes of this study. It is important to note that while statistical dependencies discovered using our approach imply directed functional connectivity, these do not necessarily imply direct anatomical connectivity: an edge in the structure could reflect indirect anatomical connectivity.

MTwDBN based models provide a quantitative description of information flow pattern in an ensemble. In this study, they provide the first structural description of the attention modulation of dependencies in cortical space and time in a compartmentalized network, such as the laminar cortical network. They allow us to quantify the unique contributions of activity history and network interactions to information processing in such a neural ensemble. We expect this framework to extend to neuronal ensembles in other parts of the nervous system, and to play an important role in revealing flexible information processing principles in the brain.

METHODS SUMMARY

Synthetic Data Dataset for Figure 1 was constructed by simulating a probabilistic spiking network with causal and shared connectivity among 8 neural variables**.** Dataset for evaluating the MTwDBN pipeline (Fig 2) was generated by simulating a network of stochastically spiking excitatory and inhibitory neurons.

Electrophysiological Data 16-channel laminar probes were used to record data from visual area V4 of 2 macaque monkeys as they performed an attention demanding task over 30 sessions total [35]. The probe recorded single units with overlapping receptive fields across the depth of the cortex. Single units were classified using peak-to-trough duration.

Behavior Monkeys were trained to perform an attention-demanding change detection task [35].

Fitting DBN graph structure was fitted to 200 ms of visual stimulus flashes. Data was prepared using 15 ms bins to fit a DBN with either 21 (3 laminar populations, 7 lags) or 42 nodes (3 lamina x 2 waveform types, 7 lags). Bootstrap methods were used to generate edge weights or confidence measures of edges discovered from the data.

186 **FIGURE CAPTIONS**

187 **Figure 1 Pairwise- and network-model parameters as a function of unique vs. shared**
188 **dependencies**. **a** A synthetic ensemble of eight neural variables with two kinds of dependencies
189 – unique or shared – between seven source variables (black) and one target variable (cyan). All
190 interactions are excitatory. Strength of dependencies is determined by model parameters P_{unique}
191 and P_{shared} (see SI Methods). **b** Normalized total mutual information, measured by uncertainty
192 coefficient, as a function of the sum of model parameters (P_{unique}, P_{shared}) that varied unique and
193 shared components of mutual information in a monotonic way (Fig S1c-d). **c** Coefficients of
194 pairwise model (univariate logistic regression) as a function of P_{unique} and P_{shared}. White arrow
195 provides a visual guide for direction of highest change in coefficients. **d** Coefficients of network
196 model (multivariate LASSO regression) as a function of P_{unique} and P_{shared}. White arrow provides
197 a visual guide for direction of highest change in coefficients. **e** Schema for utilizing pairwise and
198 network methods for the estimation of total (black) and unique (green) information modulation
199 respectively, and to infer the modulation of shared information (purple). Shaded blocks indicate
200 indeterminate modulation direction of shared information in the network.

201

202 **Figure 2 DBN based estimation of multi-timescale weighted unique dependency. a** Analysis
203 flow for multi-timescale weighted DBN (MTwDBN) model fitting. **b** Edge weight of MTwDBN as a
204 function of connection weight in a 2-population simulated network using the pipeline in **a**. **c** Spiking
205 activity of 6 subpopulations in a simulated laminar network. Connectivity is visualized in the
206 overlaid schematic. **d** Directed dependencies (edge in the graph) in the simulated network in **c**,
207 estimated using MTwDBN fitting. **e** Summary graph of dependencies across all timescales from
208 **d**. **f** F score (harmonic mean of precession and recall of dependency structure) as a function of
209 % of population observed. F score was estimated for shuffle corrected weighted DAGs

210 (MTwDBN), weighted DAGs with fixed threshold (FT), or unweighted DAGs. **g** DBN decoder
211 accuracy with different sizes of MTwDBN DAGs. Decoders were trained to predict population
212 activities using a subsample of shuffle corrected edges (see SI Methods). Graph edges for the
213 decoder were sampled from the learned structure either in an unbiased fashion or biased with the
214 edge weights.
215
216 **Figure 3 Modulation of dependencies in a V4 laminar network across attention conditions.**
217 **a** Experimental protocol: Paired Gabor stimuli with different contrasts (see Methods); one stimulus
218 was presented inside the receptive fields (RFs) of the recorded neurons and the other at an
219 equally eccentric location across the vertical meridian. Attention was cued either to the neurons'
220 RFs ("IN") or to the location in the contralateral visual hemifield ("AWAY"). Orientation of one of
221 the two stimuli changed at a random time. Monkey was rewarded for detecting the change by
222 making a saccade to the corresponding location. Task difficulty was controlled by the magnitude
223 of orientation change. **b** Recording approach: laminar recordings in visual area V4. **c** Neural
224 populations used for MTwDBN analysis. Current source density analysis identified different layers
225 (*superficial*, *input*, *deep*), and isolated single units were assigned to one of these layers (see SI
226 Methods). **d** *Top*: Average MTwDBN-based modulation (green) of all unique dependencies
227 between the laminar populations. Modulation of the same dependencies as estimated by logistic
228 regression (black). *Bottom*: PID framework-based estimated modulation sign of shared
229 dependencies (see schema in Fig 1e). Thicker line along the time axis indicates the timescales
230 of attentional modulation in prior studies[38,39]. Error bars indicate 95% confidence intervals. **e** Sign
231 of average modulation of unique dependencies between layers (bi-directionally). **f** Sign of average
232 modulation of shared dependencies within layers. **g** Sign of average modulation of unique
233 dependencies within layers. **h** Summary of dependency modulation pattern. **i** Neural populations
234 used for laminar MTwDBN analysis. Isolated single units were classified as broad and narrow

based on peak-to-trough duration in their average spike shape (see SI Methods). **j-n** Same as **d-h**, but for populations shown in **i**. I: input layer; S: superficial layer; *M1*, *M2*: subject-wise dependencies; *broad*, *narrow*: cell-class specific dependencies. See Fig S4 for modulation indices in **e-g**, **k-n**.

Figure 4 Modulation of dependencies in a V4 laminar network across behavioral outcomes at perceptual threshold. a Example session showing performance as a function of task difficulty. (orange box: threshold orientation change at which the animal was equally likely to correctly detect (Hit) or fail to detect (Miss) the change). **b** Laminar populations used for multi-lag analysis. **c** Modulation magnitude (top) and sign (bottom) of all unique (green) and total (black) laminar dependencies in **b** across Hits and Misses at perceptual threshold. Estimated modulation sign of shared dependencies (bottom, see Fig 1e). **d** Modulation sign of between (BL) and within (WL) layer dependencies. See Fig S5 for modulation indices. **e** Summary of laminar dependency modulation pattern.

Figure S1 Information decomposition in a multi-variate system

a Partial information decomposition (PID) framework[13,14] based definition of types of information that multiple sources can have about a target.

b Application of pairwise and network-based statistical models for approximate information decomposition in a multivariate system. Panel on the right illustrates interpretation of the modulation of these dependencies using the PID framework.

c, d Reduction in the proportion of total entropy (or information fraction) as a function of parameters (P_{unique}, P_{shared}) that control unique and shared information in the model. For the sake

258 of computational efficiency, information fraction estimation as a function of P_{shared} (d) was
259 performed using a subset of variables in the simulated network.
260
261 **Figure S2 Additional MTwDBN performance metric for synthetic data**
262 Recall, precision and F score measures for weighted DAGs in Fig 2d as a function of number of
263 lags.
264
265 **Figure S3 Laminar recordings in area V4**
266 **a** Stacked contour plot showing spatial receptive fields (RFs) along the laminar probe from an
267 example session. The RFs are well aligned, indicating perpendicular penetration down a cortical
268 column. Zero depth represents the center of the input layer as estimated with current source
269 density (CSD) analysis. **b** CSD displayed as a colored map. The x-axis represents time from
270 stimulus onset; the y-axis represents cortical depth. The CSD map has been spatially smoothed
271 for visualization. **c** An example trial showing single-unit activity across the cortical depth in the
272 attend-in condition. The time axis is referenced to the appearance of the fixation spot. Spikes
273 (vertical ticks) in each recording channel come from the single unit with the highest spike rate in
274 this trial. The gray boxes depict stimulus presentation epochs. In this particular trial, 8 sample
275 stimuli with different contrasts were presented, followed by a target stimulus flash with an
276 orientation change that the monkey responded to correctly. Spike waveforms for two example
277 narrow (cyan) and broad (orange) single units are shown.
278
279 **Figure S4 Modulation of dependencies in a V4 laminar network across attention**
280 **conditions.** MTwDBN-based modulation (green) of all unique dependencies between the laminar
281 populations. Modulation of the same dependencies as estimated by logistic regression (black).
282 Open circles indicate no significant edges for a given time lag. Schematic at the top of every

column depicts the populations used for identifying laminar dependency structure within (left) and between (right) cortical layers. *broad, narrow*: cell-class specific populations identified by spike shape (see SI Methods).

Figure S5 Modulation of dependencies in a V4 laminar network across behavioral outcomes at perceptual threshold. MTwDBN-based modulation (green) of all unique dependencies between the laminar populations. Modulation of the same dependencies as estimated by logistic regression (black). Schematic at the top of every column depicts the populations used for identifying laminar dependency structure within (left) and between (right) cortical layers.

AUTHOR CONTRIBUTIONS

AD and MPJ conceptualized the project. ASN collected the electrophysiological data. AD and MPJ generated synthetic data. AGS and AD analyzed the data. MPJ supervised the project. AGS, AD, ASN and MPJ wrote the manuscript.

ACKNOWLEDGEMENTS

This research was supported by NIH R00 EY025026, NIH R21 MH126072 and SFARI 875855 to MPJ, NARSAD Young Investigator Grant, Ziegler Foundation Grant, Yale Orthwein Scholar Funds, NIH R21 MH126072 and SFARI 875855 to ASN, NSF GRFP fellowship to AGS and by NEI core grant for vision research P30 EY026878 to Yale University. We thank Steve Chang and Weikang Shi for helpful comments on the manuscript.

REFERENCES

1 Petersen, S. E. & Posner, M. I. The attention system of the human brain: 20 years after. *Annual Review of Neuroscience* **35**, 73-89 (2012). https://doi.org:10.1146/annurev-neuro-062111-150525

2 Ruff, D. A. & Cohen, M. R. Attention Increases Spike Count Correlations between Visual Cortical Areas. *J Neurosci* **36**, 7523-7534 (2016). https://doi.org:10.1523/JNEUROSCI.0610-16.2016

3 Briggs, F., Mangun, G. R. & Usrey, W. M. Attention enhances synaptic efficacy and the signal-to-noise ratio in neural circuits. *Nature* **499**, 476-480 (2013). https://doi.org:10.1038/nature12276

4 Womelsdorf, T. & Fries, P. The role of neuronal synchronization in selective attention. *Current opinion in neurobiology* **17**, 154-160 (2007). https://doi.org:10.1016/j.conb.2007.02.002

5 Bosman, C. A. *et al.* Attentional stimulus selection through selective synchronization between monkey visual areas. *Neuron* **75**, 875-888 (2012). https://doi.org:10.1016/j.neuron.2012.06.037

6 Gregoriou, G. G., Gotts, S. J., Zhou, H. & Desimone, R. High-frequency, long-range coupling between prefrontal and visual cortex during attention. *Science* **324**, 1207-1210 (2009). https://doi.org:10.1126/science.1171402

7 Zohary, E., Shadlen, M. N. & Newsome, W. T. Correlated neuronal discharge rate and its implications for psychophysical performance. *Nature* **370**, 140-143 (1994). https://doi.org:10.1038/370140a0

8 Mitchell, J. F., Sundberg, K. A. & Reynolds, J. H. Spatial attention decorrelates intrinsic activity fluctuations in macaque area V4. *Neuron* **63**, 879-888 (2009). https://doi.org:10.1016/j.neuron.2009.09.013

9 Cohen, M. R. & Maunsell, J. H. R. Attention improves performance primarily by reducing interneuronal correlations. *Nature Neuroscience* **12**, 1594-1600 (2009). https://doi.org:10.1038/nn.2439

10 Desimone, R. & Duncan, J. Neural mechanisms of selective visual attention. *Annual Review of Neuroscience* **18**, 193-222 (1995).

11 McAdams, C. & Maunsell, J. Effects of Attention on Orientation-Tuning Functions of Single Neurons in Macaque Cortical Area V4. *J Neurosci* **19**, 431-441 (1999).

12 Reynolds, J., Pasternak, T. & Desimone, R. Attention increases sensitivity of V4 neurons. *Neuron* **26**, 703-714 (2000).

13 Wibral, M., Priesemann, V., Kay, J. W., Lizier, J. T. & Phillips, W. A. Partial information decomposition as a unified approach to the specification of neural goal functions. *Brain Cogn* **112**, 25-38 (2017). https://doi.org:10.1016/j.bandc.2015.09.004

14 Williams, P. L. & Beer, R. D. Nonnegative decomposition of multivariate information. *arXiv preprint arXiv:1004.2515* (2010).

15 Fiebelkorn, I. C., Pinsk, M. A. & Kastner, S. in *Neuron* Vol. 99 842-853.e848 (2018).

16 Helfrich, R. F. *et al.* in *Neuron* Vol. 99 854-865.e855 (2018).

17 Fiebelkorn, I. C., Saalmann, Y. B. & Kastner, S. in *Current Biology* Vol. 23 2553-2558 (Elsevier, 2013).

18 Douglas, R. J. & Martin, K. A. C. Neuronal circuits of the neocortex. *Annual Review of Neuroscience* **27**, 419-451 (2004). https://doi.org:10.1146/annurev.neuro.27.070203.144152

19 Douglas, R. J. & Martin, K. A. C. Recurrent neuronal circuits in the neocortex. *Current biology : CB* **17**, R496-500 (2007). https://doi.org:10.1016/j.cub.2007.04.024

20 D'Souza, R. D. & Burkhalter, A. in *Front Neuroanat* Vol. 11 71 (2017).

21 Gattass, R., Galkin, T. W., Desimone, R. & Ungerleider, L. G. in *J Comp Neurol* Vol. 522 1941-1965 (John Wiley & Sons, Ltd, 2014).

22 Ungerleider, L. G., Galkin, T. W., Desimone, R. & Gattass, R. Cortical connections of area V4 in the macaque. *Cerebral cortex (New York, NY : 1991)* **18**, 477-499 (2008). https://doi.org:10.1093/cercor/bhm061

23 Koller, D. & Friedman, N. *Probabilistic graphical models: principles and techniques*. (MIT press, 2009).

24 Murphy, K. P. & Russell, S. Dynamic bayesian networks: representation, inference and learning. (2002).

25 Smith, V. A., Jarvis, E. D. & Hartemink, A. J. Evaluating functional network inference using simulations of complex biological systems. *Bioinformatics* **18**, S216-S224 (2002).

26 Zhang, L., Samaras, D., Alia-Klein, N., Volkow, N. & Goldstein, R. in *Advances in neural information processing systems.* 1593-1600.

27 Rajapakse, J. C. & Zhou, J. Learning effective brain connectivity with dynamic Bayesian networks. *Neuroimage* **37**, 749-760 (2007).

28 Smith, V. A., Yu, J., Smulders, T. V., Hartemink, A. J. & Jarvis, E. D. Computational inference of neural information flow networks. *PLoS computational biology* **2** (2006).

29 Eldawlatly, S., Zhou, Y., Jin, R. & Oweiss, K. G. On the use of dynamic Bayesian networks in reconstructing functional neuronal networks from spike train ensembles. *Neural Comput* **22**, 158-189 (2010). https://doi.org:10.1162/neco.2009.11-08-900

30 Seth, A. K., Barrett, A. B. & Barnett, L. Granger causality analysis in neuroscience and neuroimaging. *J Neurosci* **35**, 3293-3297 (2015). https://doi.org:10.1523/JNEUROSCI.4399-14.2015

31 Friedman, N., Goldszmidt, M. & Wyner, A. Data analysis with Bayesian networks: A bootstrap approach. *arXiv preprint arXiv:1301.6695* (2013).

32 Levina, A. & Priesemann, V. Subsampling scaling. *Nat Commun* **8**, 15140 (2017). https://doi.org:10.1038/ncomms15140

33 Dalgleish, H. W. *et al.* How many neurons are sufficient for perception of cortical activity? *Elife* **9** (2020). https://doi.org:10.7554/eLife.58889

34 Priesemann, V., Munk, M. H. & Wibral, M. Subsampling effects in neuronal avalanche distributions recorded in vivo. *BMC Neurosci* **10**, 40 (2009). https://doi.org:10.1186/1471-2202-10-40

35 Nandy, A. S., Nassi, J. J. & Reynolds, J. H. Laminar Organization of Attentional Modulation in Macaque Visual Area V4. *Neuron* **93**, 235-246 (2017). https://doi.org:10.1016/j.neuron.2016.11.029

36 Mitchell, J. F., Sundberg, K. A. & Reynolds, J. H. Differential attention-dependent response modulation across cell classes in macaque visual area V4. *Neuron* **55**, 131-141 (2007). https://doi.org:10.1016/j.neuron.2007.06.018

37 Cohen, M. R. & Maunsell, J. H. R. Using neuronal populations to study the mechanisms underlying spatial and feature attention. *Neuron* **70**, 1192-1204 (2011). https://doi.org:10.1016/j.neuron.2011.04.029

38 Mitchell, J. F., Sundberg, K. A. & Reynolds, J. H. in *Neuron* Vol. 63 879-888 (2009).

39 Cohen, M. R. & Maunsell, J. H. R. in *Nat. Neurosci.* Vol. 12 1594-1600 (2009).

40 Pettine, W. W., Steinmetz, N. A. & Moore, T. Laminar segregation of sensory coding and behavioral readout in macaque V4. *Proc Natl Acad Sci U S A* **116**, 14749-14754 (2019). https://doi.org:10.1073/pnas.1819398116

41 McGinley, M. J., David, S. V. & McCormick, D. A. in *Neuron* Vol. 87 179-192 (2015).

42 Landau, A. N. & Fries, P. Attention samples stimuli rhythmically. *Curr Biol* **22**, 1000-1004 (2012). https://doi.org:10.1016/j.cub.2012.03.054

43 Pillow, J. W. *et al.* Spatio-temporal correlations and visual signalling in a complete neuronal population. *Nature* **454**, 995-999 (2008). https://doi.org:10.1038/nature07140

Figure 1

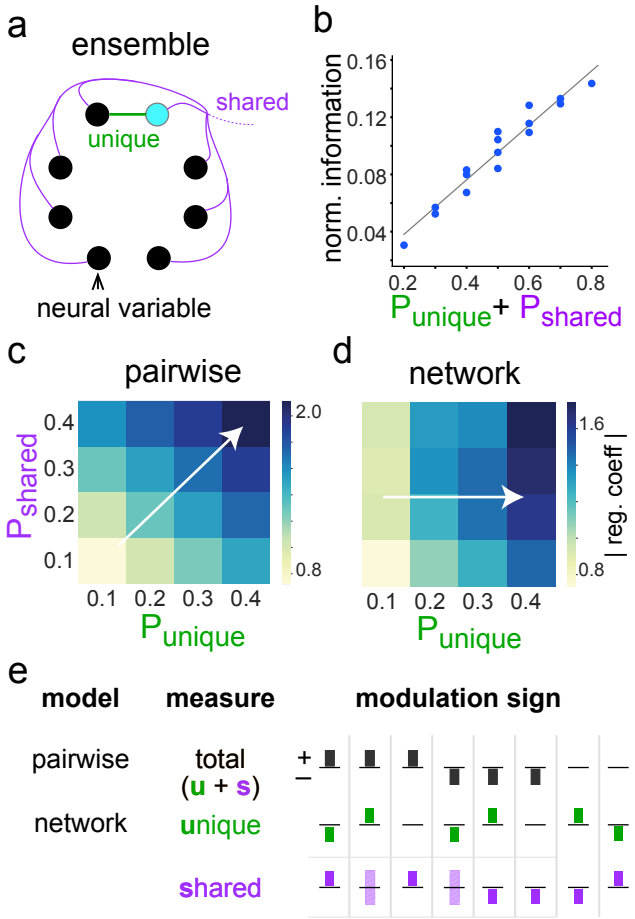

Figure 1 Pairwise- and network-model parameters as a function of unique vs. shared dependencies. a A synthetic ensemble of eight neural variables with two kinds of dependencies – unique or shared – between seven source variables (black) and one target variable (cyan). All interactions are excitatory. Strength of dependencies is determined by model parameters P_{unique} and P_{shared} (see SI Methods). **b** Normalized total mutual information, measured by uncertainty coefficient, as a function of the sum of model parameters (P_{unique} ,P_{shared}) that varied unique and shared components of mutual information in a monotonic way (Fig S1c-d). **c** Coefficients of pairwise model (univariate logistic regression) as a function of P_{unique} and P_{shared}. White arrow provides a visual guide for direction of highest change in coefficients. **d** Coefficients of network model (multivariate LASSO regression) as a function of P_{unique} and P_{shared}. White arrow provides a visual guide for direction of highest change in coefficients. **e** Schema for utilizing pairwise and network methods for the estimation of total (black) and unique (green) information modulation respectively, and to infer the modulation of shared information (purple). Shaded blocks indicate indeterminate modulation direction of shared information in the network.

Figure 2

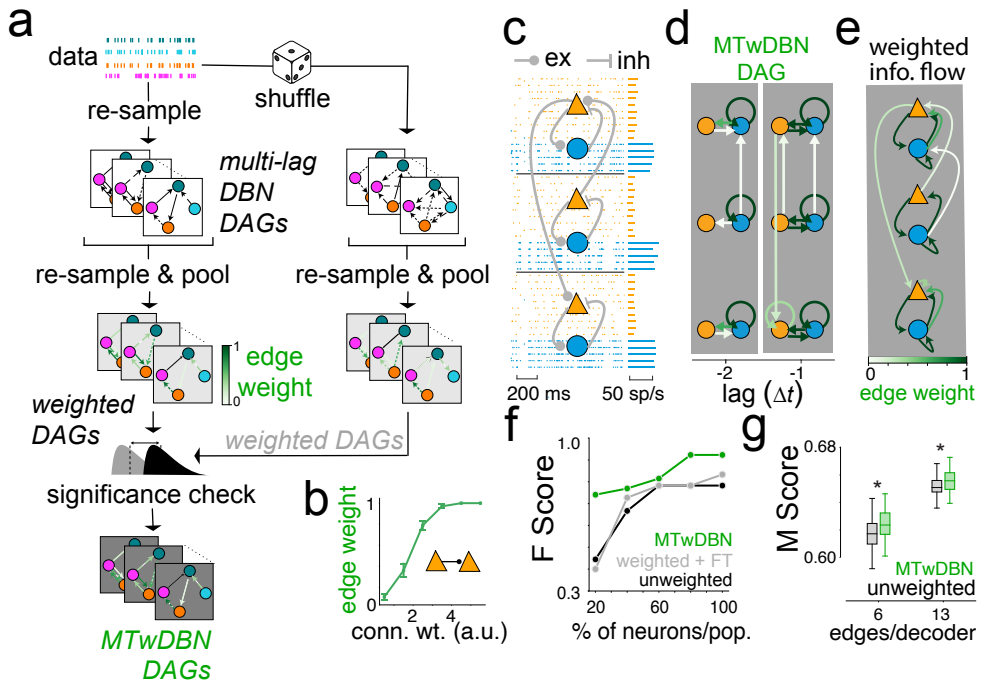

Figure 2 DBN based estimation of multi-timescale weighted unique dependency. a Analysis flow for multi-timescale weighted DBN (MTwDBN) model fitting. **b** Edge weight of MTwDBN as a function of connection weight in a 2-population simulated network using the pipeline in **a**. **c** Spiking activity of 6 subpopulations in a simulated laminar network. Connectivity is visualized in the overlaid schematic. **d** Directed dependencies (edge in the graph) in the simulated network in **c**, estimated using MTwDBN fitting. **e** Summary graph of dependencies across all timescales from **d**. **f** F score (harmonic mean of precession and recall of dependency structure) as a function of % of population observed. F score was estimated for shuffle corrected weighted DAGs (MTwDBN), weighted DAGs with fixed threshold (FT), or unweighted DAGs. **g** DBN decoder accuracy with different sizes of MTwDBN DAGs. Decoders were trained to predict population activities using a subsample of shuffle corrected edges (see SI Methods). Graph edges for the decoder were sampled from the learned structure either in an unbiased fashion or biased with the edge weights.

Figure 3

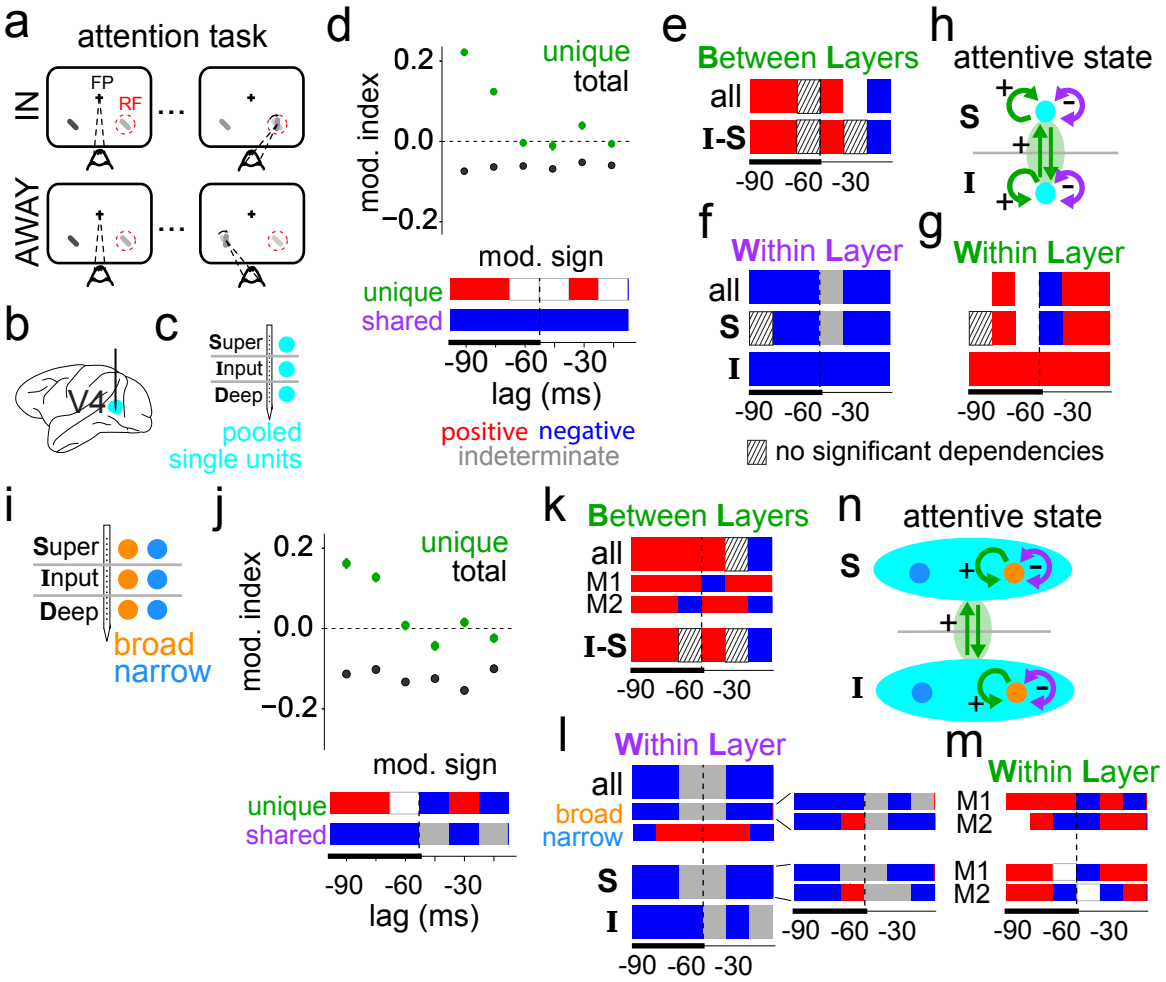

Figure 3 Modulation of dependencies in a V4 laminar network across attention conditions. **a** Experimental protocol: Paired Gabor stimuli with different contrasts (see Methods); one stimulus was presented inside the receptive fields (RFs) of the recorded neurons and the other at an equally eccentric location across the vertical meridian. Attention was cued either to the neurons' RFs ("IN") or to the location in the contralateral visual hemifield ("AWAY"). Orientation of one of the two stimuli changed at a random time. Monkey was rewarded for detecting the change by making a saccade to the corresponding location. Task difficulty was controlled by the magnitude of orientation change. **b** Recording approach: laminar recordings in visual area V4. **c** Neural populations used for MTwDBN analysis. Current source density analysis identified different layers (*superficial*, *input*, *deep*), and isolated single units were assigned to one of these layers (see SI Methods). **d** *Top*: Average MTwDBN-based modulation (green) of all unique dependencies between the laminar populations. Modulation of the same dependencies as estimated by logistic regression (black). *Bottom*: PID framework-based estimated modulation sign of shared dependencies (see schema in Fig 1e). Thicker line along the time axis indicates the timescales of attentional modulation in prior studies[38,39]. Error bars indicate 95% confidence intervals. **e** Sign of average modulation of unique dependencies between layers (bi-directionally). **f** Sign of average modulation of shared dependencies within layers. **g** Sign of average modulation of unique dependencies within layers. **h** Summary of dependency modulation pattern. **i** Neural populations used for laminar MTwDBN analysis. Isolated single units were classified as broad and narrow based on peak-to-trough duration in their average spike shape (see SI Methods). **j-n** Same as **d-h**, but for populations shown in **i**. I: input layer; S: superficial layer; *M1*, *M2*: subject-wise dependencies; *broad*, *narrow*: cell-class specific dependencies. See Fig S4 for modulation indices in **e-g**, **k-n**.

Figure 4

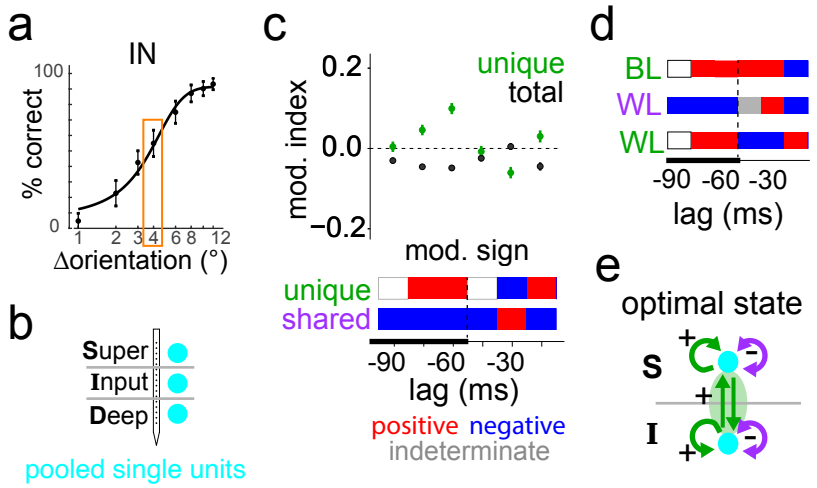

Figure 4 Modulation of dependencies in a V4 laminar network across behavioral outcomes at perceptual threshold. **a** Example session showing performance as a function of task difficulty. (orange box: threshold orientation change at which the animal was equally likely to correctly detect (Hit) or fail to detect (Miss) the change). **b** Laminar populations used for multi-lag analysis. **c** Modulation magnitude (top) and sign (bottom) of all unique (green) and total (black) laminar dependencies in **b** across Hits and Misses at perceptual threshold. Estimated modulation sign of shared dependencies (bottom, see Fig 1e). **d** Modulation sign of between (BL) and within (WL) layer dependencies. See Fig S5 for modulation indices. **e** Summary of laminar dependency modulation pattern.

Figure S1

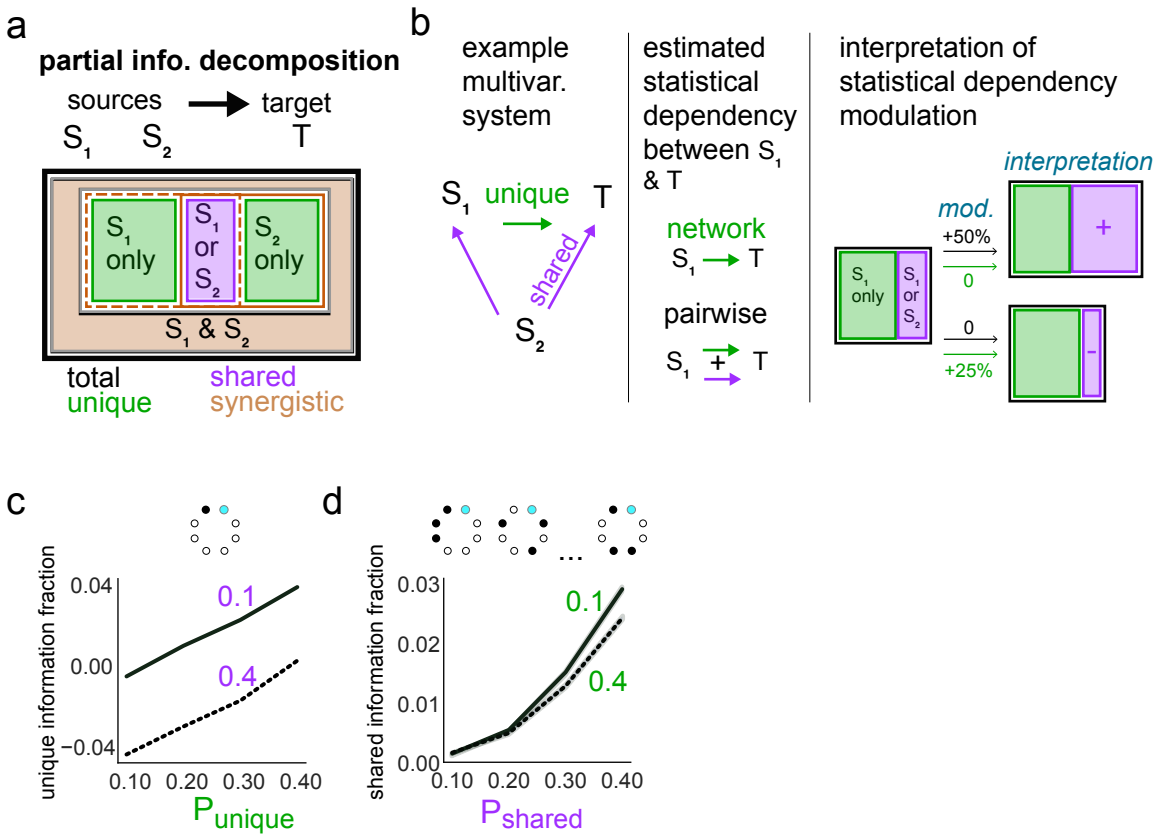

Figure S1 Information decomposition in a multi-variate system

a Partial information decomposition (PID) framework[13,14] based definition of types of information that multiple sources can have about a target.

b Application of pairwise and network-based statistical models for approximate information decomposition in a multivariate system. Panel on the right illustrates interpretation of the modulation of these dependencies using the PID framework.

c, d Reduction in the proportion of total entropy (or information fraction) as a function of parameters (P_{unique},P_{shared}) that control unique and shared information in the model. For the sake of computational efficiency, information fraction estimation as a function of P_{shared} (**d**) was performed using a subset of variables in the simulated network.

Figure S2

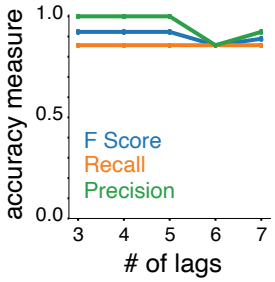

Figure S2 Additional MTwDBN performance metric for synthetic data
Recall, precision and F score measures for weighted DAGs in Fig 2d as a function of number of lags.

Figure S3

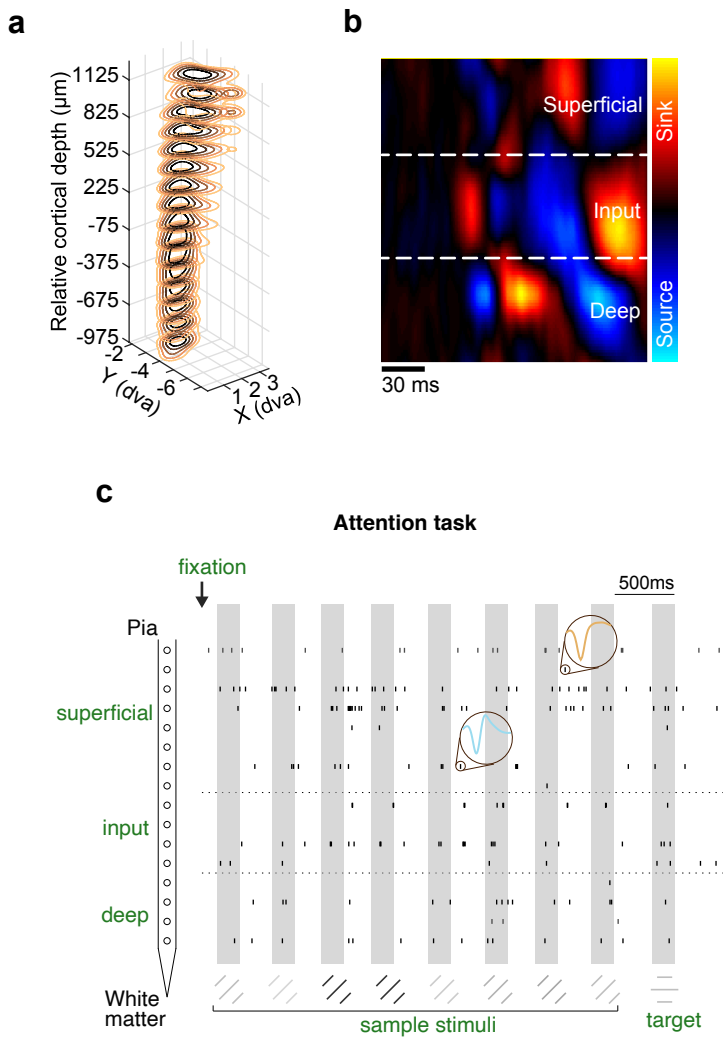

Figure S3 Laminar recordings in area V4

a Stacked contour plot showing spatial receptive fields (RFs) along the laminar probe from an example session. The RFs are well aligned, indicating perpendicular penetration down a cortical column. Zero depth represents the center of the input layer as estimated with current source density (CSD) analysis. **b** CSD displayed as a colored map. The x-axis represents time from stimulus onset; the y-axis represents cortical depth. The CSD map has been spatially smoothed for visualization. **c** An example trial showing single-unit activity across the cortical depth in the attend-in condition. The time axis is referenced to the appearance of the fixation spot. Spikes (vertical ticks) in each recording channel come from the single unit with the highest spike rate in this trial. The gray boxes depict stimulus presentation epochs. In this particular trial, 8 sample stimuli with different contrasts were presented, followed by a target stimulus flash with an orientation change that the monkey responded to correctly. Spike waveforms for two example narrow (cyan) and broad (orange) single units are shown.

Figure S4

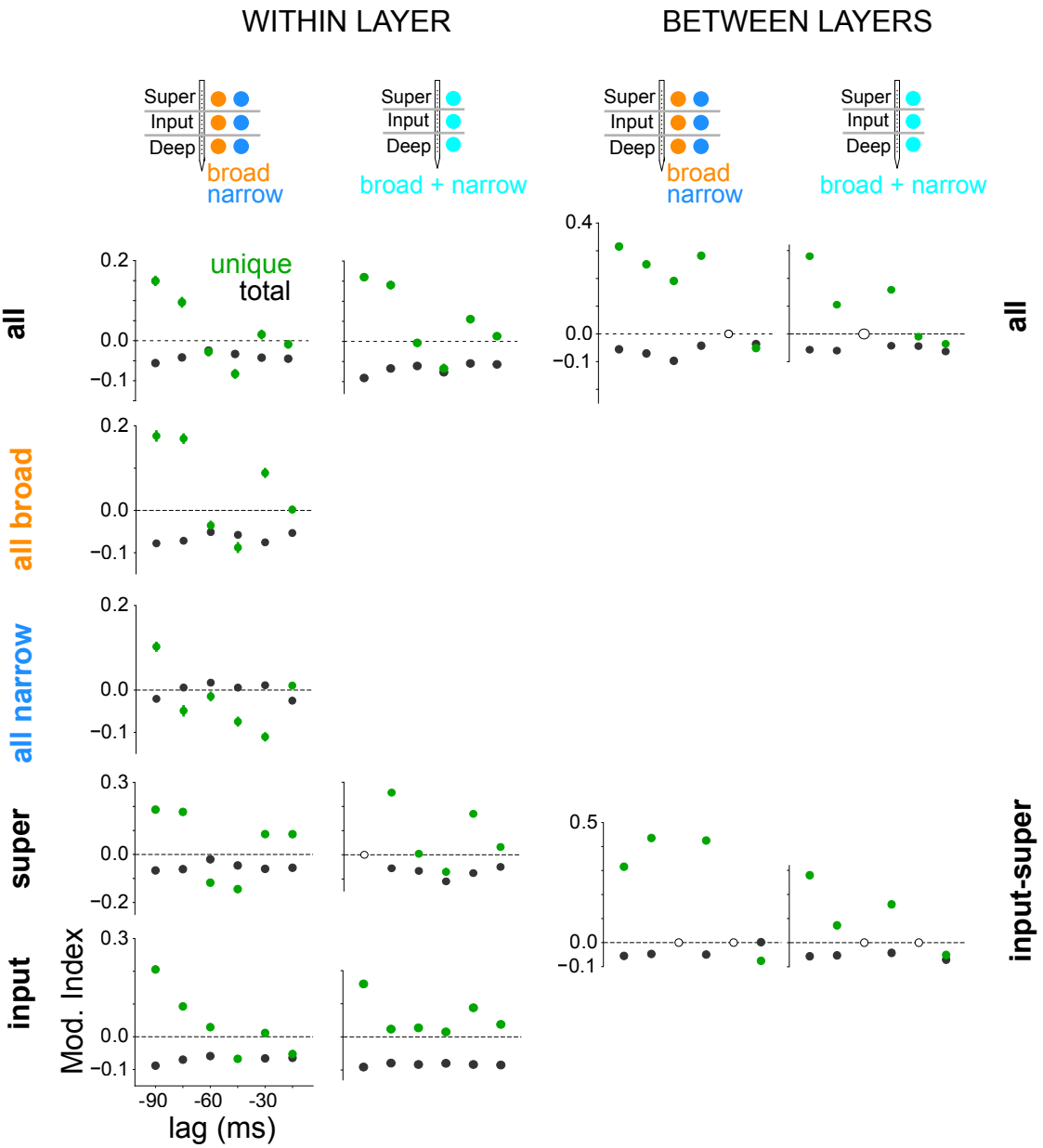

Figure S4 Modulation of dependencies in a V4 laminar network across attention conditions. MTwDBN-based modulation (green) of all unique dependencies between the laminar populations. Modulation of the same dependencies as estimated by logistic regression (black). Open circles indicate no significant edges for a given time lag. Schematic at the top of every column depicts the populations used for identifying laminar dependency structure within (left) and between (right) cortical layers. *broad*, *narrow*: cell-class specific populations identified by spike shape (see SI Methods).

Figure S5

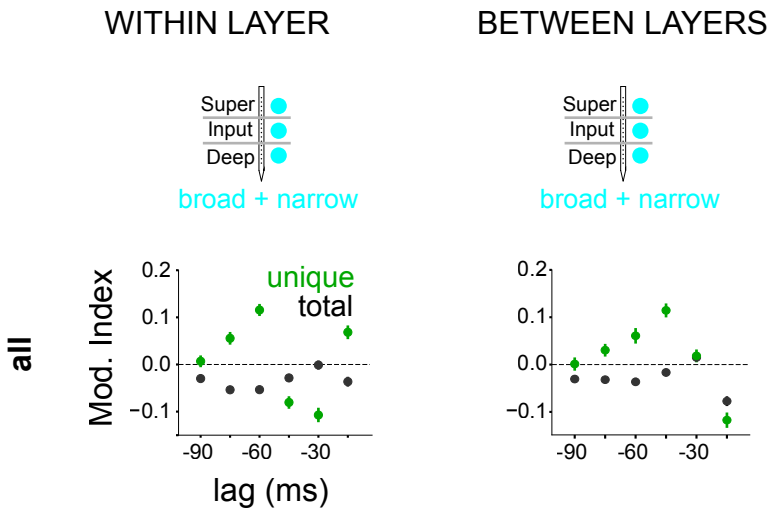

Figure S5 Modulation of dependencies in a V4 laminar network across behavioral outcomes at perceptual threshold. MTwDBN-based modulation (green) of all unique dependencies between the laminar populations. Modulation of the same dependencies as estimated by logistic regression (black). Schematic at the top of every column depicts the populations used for identifying laminar dependency structure within (left) and between (right) cortical layers.